



Molecular recognition and effects of a benzothiazole derivative targeting the *MYC* G-quadruplex

Xiao Ni¹, Xiao-Dong Hu¹, Wei Long², Wenxian Lan³, Chunxi Wang¹, Wing-Leung Wong ^{©2,*}, Chunvang Cao ^{©1,*}

¹State Key Laboratory of Chemical Biology, Shanghai Institute of Organic Chemistry, University of Chinese Academy of Sciences, Chinese Academy of Sciences, Shanghai 200032, China

²State Key Laboratory of Chemical Biology and Drug Discovery, Department of Applied Biology and Chemical Technology, The Hong Kong Polytechnic University, Kowloon, Hong Kong SAR 999077, China

³The Core Facility Center of CAS Center for Excellence in Molecular Plant Sciences, Institute of Plant Physiology and Ecology, Chinese Academy of Sciences, Shanghai 200032, China

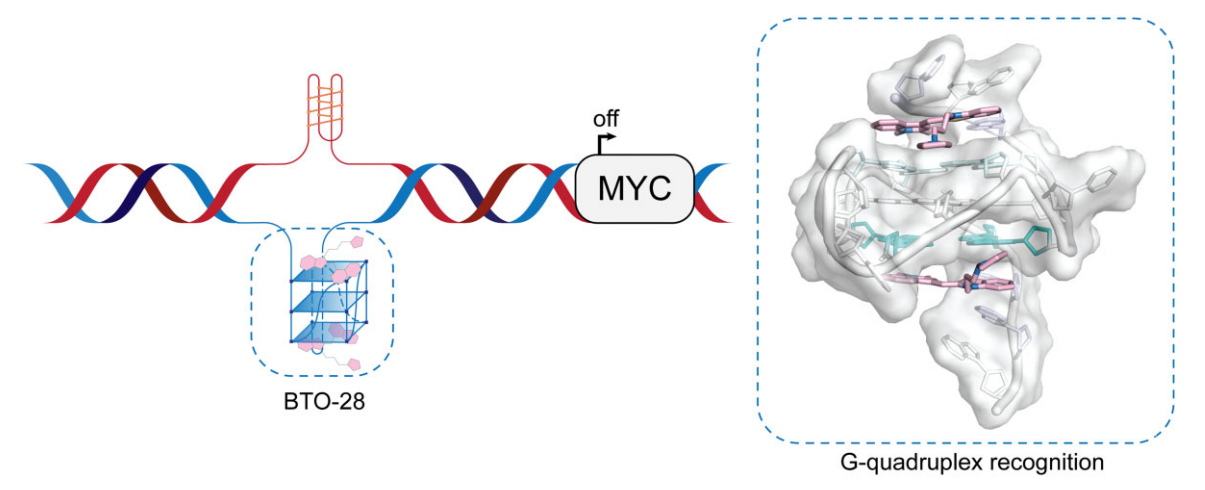
*To whom correspondence should be addressed. Email: ccao@mail.sioc.ac.cn

Correspondence may also be addressed to Wing-Leung Wong. Email: wing.leung.wong@polyu.edu.hk

Abstract

Small-molecule intervention and stabilization of G-quadruplexes (G4s) have been investigated for the potential as therapeutic approaches. MYC plays diverse roles in cellular functions, making it a highly desirable yet challenging target. One promising strategy includes DNA G4 structures, which mediate transcriptional control over MYC in the presence of small-molecule ligands. Unraveling the effects of these ligands on G4 stability and functionality is seldom achieved yet essential for designing potent ligands against these intractable targets. This study introduces BTO-28, a benzothiazole-based ligand that binds with high affinity to the MYC G4. In vitro experiments, NMR analysis, and intracellular assays collectively indicate that BTO-28 potentially downregulates MYC transcription through a G4-mediated mechanism. Structural determination of the 2:1 benzothiazole-MYC G4 complex provides insights into unexpected molecular interactions, highlighting for the first time a unique hydrogen-bonding pattern involving the nucleobase surrogate and flanking residues. The protonated pyrrolidine side chains of BTO-28 reorient to form hydrogen bonding with the external G-tetrad, establishing a previously uncharacterized ligand–G4 interface. This work advances the rational design of G4-binding ligands and clarifies the molecular basis underlying MYC recognition.

Graphical abstract



Introduction

G-quadruplexes (G4s) are noncanonical four-stranded DNA structures that play regulatory roles in key genomic regions [1]. These structures originate from guanine-rich sequences under physiological conditions [2], and their folding is dynamic in live cells [3]. They are commonly located in human telomeres [4], the promoters of genes such as MYC

[5, 6], EGFR [7], and KIT [8], as well as untranslated regions [9]. Using high-resolution techniques for genome-wide analysis, researchers have uncovered a more extensive and diverse set of G4 structures than previously recognized [10, 11]. G4s are emerging as promising molecular targets for therapeutic interventions, with notable potential in targeting MYC and additional oncogenes [12]. The oncogene MYC

coordinates critical transcriptional programs involved in the initiation and maintenance of tumorigenesis [13]. Elevated expression of MYC is associated with more than half of human cancers through multiple mechanisms, including gene amplification, chromosomal translocation, and mutation of upstream signaling pathways [14]. Endogenous MYC is essential for maintenance of solid tumor and its inhibition has demonstrated potential therapeutic value [15]. MYC's pleiotropic roles in diverse cellular processes making it a coveted therapeutic target, but several technical challenges, especially the intrinsically disordered binding region [16], have so far hindered the development of MYC inhibitory drugs. A significant amount of medicinal researches have focused on targeting MYC, employing a variety of strategies to address this challenging target [17, 18]. Noteworthy efforts include disruption of MYC-MAX heterodimerization, which inhibits Ebox DNA binding and promotes the degradation of MYC [19, 20]. Recent entry of OMO-103 into clinical trials has demonstrated both safety and preliminary antitumor activity [21]. Further studies are ongoing to assess its therapeutic potential.

An alternative approach has been explored to perturb the transcriptional activity of MYC by targeting its promoter region. MYC dysregulation in most human cancers is typically not due to mutations in the MYC gene itself but rather a consequence of its activation by upstream oncogenic signaling pathways [22]. Negative supercoiling induced by MYC transcription has been shown to drive topological changes from duplex DNA to non-B-DNA structures [23]. Some transcription factors, such as SP1, activate transcription by binding to the duplex form of Nuclease Hypersensitive Element III₁ (NHE III₁) [24]. The formation of G-quadruplexes within this element sequesters SP1 and other proteins, consequently acting as a transcriptional repressor of MYC expression [25–27]. Genetic abrogation of the folding of endogenous G4 structures leads to a reduction in transcription factor recruitment in cells [28]. Endogenous G4 formation at gene promoters in live cells has been demonstrated using G4-selective antibodies and smallmolecule probes [29]. However, the functional role of G4 in transcription remains unresolved. Molecules that selectively recognize distinct DNA folds in the human genome could be used to perturb gene expression or regulate signaling pathways [30–32], offering potential as therapeutic agents. Further credence has been given to the strategy of targeting G4 structures by the recent investigation of CX-5461 in phase I and II clinical trials for patients with BRCA1-/BRCA2-deficient tumors [33, 34]. Proposed mechanisms for selective inhibition of CX-5461 include stabilizing G4 structures and impeding replication fork progression [35]. The mutagenic effects of CX-5461 in normal cells raise safety concerns [33] and underscore the need for a deeper understanding of G4-ligand interactions in the drug development. To unravel the mechanistic role of G4 formation in gene regulation, it is essential to study G4-interacting ligands, especially those that may modulate gene expression.

The MYC G-quadruplex, formed in the NHE III₁ region of the MYC oncogene promoter (Fig. 1A), is essential for regulating multiple cellular processes [36]. Pioneering studies, including the work by Yang and coworkers, identified the major G4 structure of this regulatory element using nuclear magnetic resonance (NMR) spectroscopy [37], with subsequent validation by X-ray crystallography [38]. In a recent structural investigation, a platinum(II) compound was found to stabilize

the MYC G-quadruplex in successive stages and inhibit MYC transcription [39]; the work highlights NMR as an effective method for probing ligand–G4 interactions. Our study focuses on the NHE III₁ element from the MYC promoter and its variants. The wild-type NHE III₁ is a 27-nucleotide sequence rich in guanine. The predominant MYC G4 structure adopts a parallel topology and comprises four consecutive 3'-runs of guanines, with G11 and G20 not contributing to the formation of the tetrads [37]. Myc2345 retains the wild-type guanine at position 20, while MYC G4 (Myc2345_T23) features a G-to-T substitution that limits the loop—isomer formation (Fig. 1B) [40]. The 2.6-Å structure of nucleolin bound to an NHE III₁-derived MYC G4 highlights loop and flanking interactions essential for G4–specific recognition both biochemically and in cells [27].

Thiazole orange is often employed as a nucleobase surrogate [41, 42], demonstrating elevated fluorescence upon incorporation into DNA. This enhancement is likely due to constrained orientations imposed by nearby base pairs [43], though the exact binding mechanism remains uncertain. The fluorescence of the thiazole orange derivatives remains unaffected by the photoinduced electron transfer quenching typically triggered by guanine [44], thereby enhancing their feasibility of targeting guanine-rich DNA sequences. Recent studies have revealed that a thiazole orange scaffold with multisite binding system can visualize endogenous G-quadruplex structures [45, 46], yet the rationale for its structural specificity remains unknown. Visualizing G4-ligand complexes at the molecular level would provide insights for the rational design of potent G4-targeting agents.

Herein, we detail the unique intermolecular binding mode of BTO-28, a high-affinity ligand of the MYC G4 (Fig. 1C). An earlier preliminary investigation reported that this ligand does not exhibit selective binding to telomeric G-quadruplexes [46]. Using NMR spectroscopy, the solution structures of the ligand in complex with MYC G4 are unambiguously determined. BTO-28 functions as a base surrogate in this unimolecular G-quadruplex, a mechanism not previously reported. Instead of simply stacking atop the external G-tetrads, the functional groups of the ligand match the hydrogen-bond arrangement of the neighboring residues while also interact with loop residues. Notably, the observed decrease in MYC transcription appears to be regulated by the NHE III₁ region through a G-quadruplex-related mechanism. Chemical and structural investigations provide molecular basis for the recognition and functional regulation of MYC G-quadruplex.

Materials and methods

Sample preparation

Unlabeled DNA sequences and 5' or 3'-Cy5 labeled oligonucleotides were obtained from Sangon Biotech. DNA samples were annealed by heating to 98°C for 10 min, followed by gradual cooling to room temperature. DNA concentration was quantified using a NanoDrop spectrophotometer (Thermo Fisher Scientific). BTO-28 was synthesized as previously described (Supplementary Figs S17 and S18) [46]. It was dissolved in dimethyl sulfoxide (DMSO) to prepare a 100 mM stock solution, then diluted to the specified working concentrations for the experiments. Water samples were prepared in a solution comprising 10% D₂O and 90% H₂O. Samples in

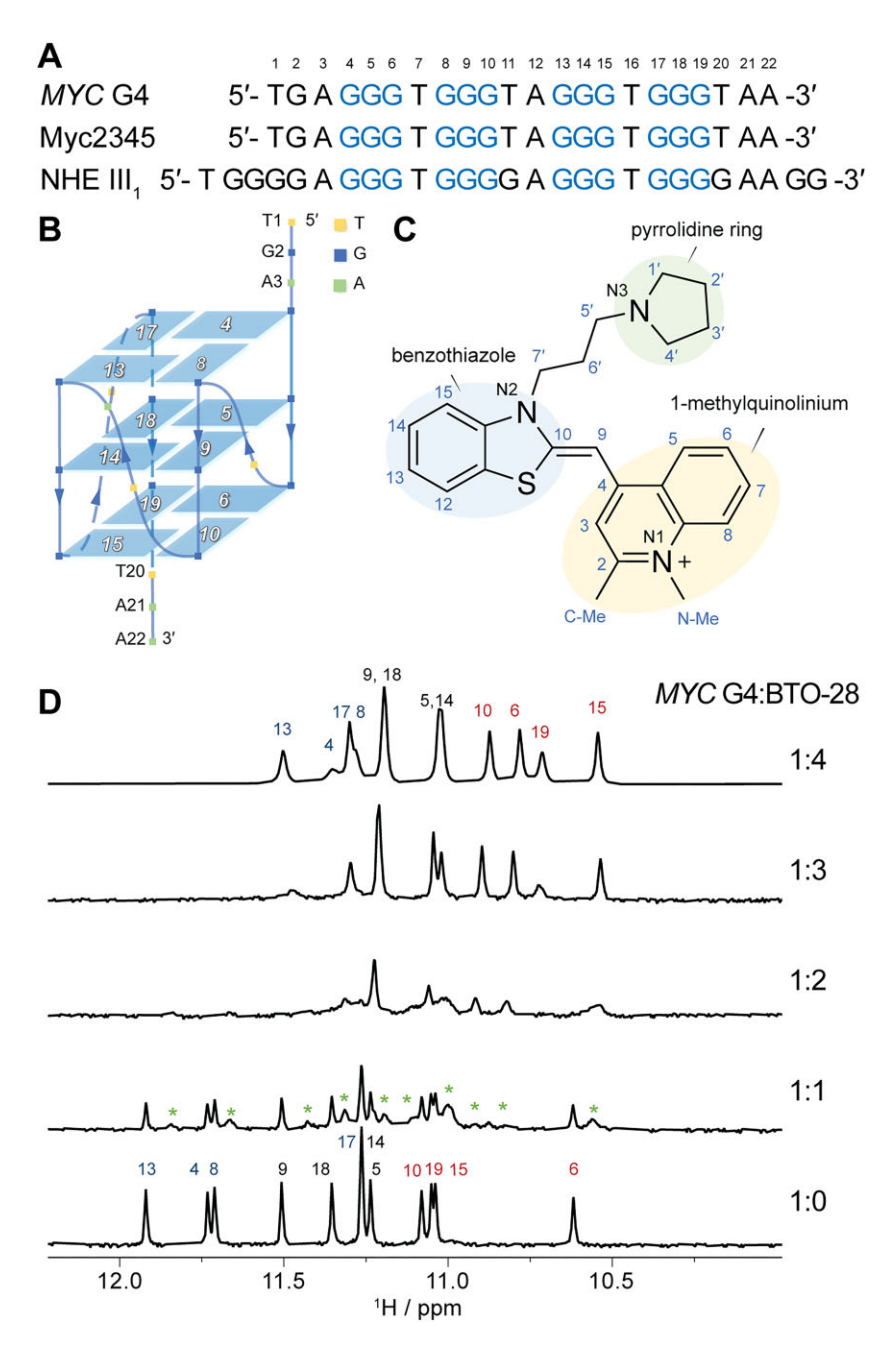


Figure 1. (A) The sequences of the NHE III $_1$ element from the *MYC* promoter and its variants. (B) Schematic representation of the *MYC* G4 folding topology. (C) Chemical structure of the benzothiazole derivative BTO-28, with its atom numbering system. (D) Expanded imino region of 1D 1 H NMR spectra during titration of BTO-28 into *MYC* G4 (100 μ M) at pH 7.4 with 10 mM K $^+$. The molar ratios of *MYC* G4 to BTO-28 are 1:0, 1:1, 1:2, 1:3, and 1:4. The imino protons are color-coded in each spectrum: blue for the 5' G-tetrad, black for the middle G-tetrad, and red for the 3' G-tetrad. New peaks arising from BTO-28–*MYC* G4 complexes are marked with green asterisks.

 D_2O were prepared by lyophilization and followed by dissolution in 99.9% D_2O (CIL).

Mass spectroscopy

DNA samples (100 μ M) were prepared in in 20 mM potassium phosphate buffer (pH 7.4) containing 80 mM KCl. The solution was heated to 98°C for 10 min, then allowed to cool slowly to room temperature. BTO-28 was added at the specified DNA:ligand ratios and incubated for 30 min. Analysis was conducted using high-performance liquid chromatography coupled to electrospray ionization mass spectrometer (HPLC–ESI–MS). Related data were processed using Xcalibur.

Circular dichroism spectroscopy

Circular dichroism (CD) experiments were performed using a JASCO-815 spectrometer (JASCO, Inc.). Samples were prepared in 20 mM Tris–HCl buffer containing 80 mM KCl at pH 7.4, to a final DNA concentration of 100 μM . The solution was heated to 98°C for 10 min, then allowed to cool slowly to room temperature. BTO-28 was added at the specified DNA:ligand ratios and incubated for 30 min. A 10-mm quartz cuvette was used, and the spectra were obtained by averaging three scans across the wavelength range of 200–400 nm. Baseline correction was performed by subtracting the buffer spectrum.

Fluorescence polarization assays

Cy5-labeled G-quadruplex constructs are prepared in 20 mM potassium phosphate buffer (pH 7.4) containing 80 mM KCl and annealed as described above. Ligand solutions are prepared by diluting compounds in the same buffer to final concentrations of 0–2 μ M. To each well, G4 was added to a final concentration of 20 nM, and the plates were incubated at room temperature for 30 min. Fluorescence polarization was subsequently measured using an EnVision microplate reader (PerkinElmer), and binding affinities were derived from single-site binding model fits in GraphPad Prism.

NMR spectroscopy

Final NMR samples contained 0.1–2.0 mM DNA in 20 mM potassium phosphate, 80 mM KCl (pH 7.4), or in the low-salt solution, 2 mM potassium phosphate, 8 mM KCl, pH 7.4 buffer. All NMR experiments were performed on an Agilent 800 MHz spectrometer. Homonuclear 2D NMR experiments, including DQF-COSY, TOCSY, and NOESY, were collected at 298 K for the benzothiazole–MYC G4 complex in both water and D₂O at 100 and 10 mM K⁺. NOESY mixing times were set from 50 to 300 ms, and the TOCSY mixing time was 70 ms. WATERGATE and excitation-sculpting were employed for water suppression. Spectra were processed using NMR-Pipe, with Sparky (UCSF) utilized cross-peak assignments and integrations.

Structure calculation

The topology parameters of BTO-28 were generated from the Automated Topology Builder server (http://atb.uq.edu.au/) and integrated into XPLOR-NIH (version 2.47). Distances between nonexchangeable protons were derived from NOESY spectra and classified into four categories: strong (1.8–2.9 Å), medium (1.8–3.5 Å), weak (1.8–5.0 Å), and very weak (1.8– 6.0 Å). The cross-peak between the thymine methyl and H6 protons (3.0 Å) served as a reference. Glycosidic torsion angles of $240 \pm 70^{\circ}$ for anti were applied based on intraresidue H8-H1' NOE intensity. The planarity restraints were applied to the G-tetrads. The structural calculations of complex were carried out using a simulated annealing protocol as previously described [47], started from the coordinate of an extended DNA chain and two BTO-28 molecules. The model was first heated to 3000 K and kept for 10 ps. The van der Waals (vdW) forces were turned off in the heating stage. The system was subsequently cooled to 25 K within 24 ps using a combined energy function composed of geometric, vdW, and NOE terms. The structure was subjected to final energy minimization for 40 ps. Among the 200 structures calculated in the last iteration, 10 structures with the lowest energies and minimal restraint violations were selected for 3D representation.

Differential scanning calorimetry

Differential scanning calorimetry (DSC) measurements were performed using an automated VP-CAP-DSC microcalorimeter (Malvern Inc., USA). G4 DNA at 100 μM was investigated both in the presence of BTO-28 at a 1:4 DNA-to-ligand molar ratio and in its absence. Temperature scans were performed from 25°C to 105°C at a rate of 1.0°C/min. A buffer-buffer scan was subtracted from each buffer-sample scan, and linear-polynomial baselines were applied to each dataset. The corrected thermograms were then normalized to the single-

stranded DNA concentration to derive molar heat capacity curves. The melting temperature ($T_{\rm m}$) was determined as the peak temperature in each thermogram.

Taq DNA polymerase stop assay

5′-d(TAATACGACTCACTATAGCAATTGCGTG)-3′ was 5′-end-labeled with FAM. The labeled primer was annealed to the DNA template (Supplementary Table S1) in 50 mM Tris (pH 7.4) using the previously described protocol [48]. The specified compounds were added to 20 nM annealed template in 50 mM Tris (pH 7.4), 1 mM MgCl₂, 5 mM dithiothreitol (DTT), dNTP mixture, and 5 U/μl *Taq* polymerase (Takara, RR001A). Samples were incubated for 40 min at 64°C for polymerase extension. The reaction was stopped by adding alkaline gel loading dye, and the samples were analyzed on a 16% denaturing polyacrylamide gel.

Cell lines

The HT-29 cells were cultured in McCoy's 5A (Gibco, 16600082) with 10% fetal bovine serum (Gibco, A5669701), 100 U/ml penicillin and 100 mg/ml streptomycin. The 293T cells were cultured in DMEM (Gibco, 11965092) with 10% fetal bovine serum, 100 U/ml penicillin and 100 mg/ml streptomycin. HK-2 cells were cultured in K-SFM (Invitrogen, 17005042) supplemented with Gentamicin/Amphotericin solution (Gibco, R01510). Cells were cultured in a Thermo Fisher Scientific (Waltham, MA) water-jacketed incubator at 37 °C with 5% CO₂.

Cell viability assays

Cell viability assay was estimated using the CellTiter blue (Promega, G8081). Cells were seeded in triplicate at a density of 8000 cells per well onto 96-well plates containing 100 μl of medium per well and incubated for 12 h. The drug, diluted in complete medium, was then added to each well. Cell viability was assessed by measuring absorbance at 590 nm using an EnVision microplate reader (PerkinElmer).

Quantitative real-time PCR

Total mRNA was isolated with a MiniBEST Universal RNA Extraction Kit (TaKaRa, 9767), and complementary DNA synthesis was performed with a PrimeScriptRT Mater Mix (TaKaRa, RR036A), per the manufacturers' instructions. Quantitative polymerase chain reaction (qPCR) analysis was conducted on a QuantStudio 6 Flex Real-Time PCR (Applied Biosystems) with TB Green Premix Ex Taq II FAST qPCR (TaKaRa, CN830S). Expression levels were quantified with the $\Delta\Delta C_t$ method and normalized to β -actin mRNA. Sequences of primers used are listed in Supplementary Table S1.

Chromatin immunoprecipitation qPCR

Approximately 1×10^8 HT-29 cells were treated with DMSO or BTO-28 (1000 nM) and cross-linked with 1% formaldehyde at 37°C for 10 min. Chromatin immunoprecipitation (ChIP) assays were performed using SimpleChIP Enzymatic Chromatin IP Kit (Cell Signaling Technology, 9003S), according to the manufacturer's instructions. Chromatin was immunoprecipitated overnight at 4°C with 2 μg of the antibody of interest. Antibody-bound complexes were subsequently isolated using ChIP-Grade Protein G Magnetic Beads (Cell Signaling Technology, 9006). Immunoprecipitated DNA

was analyzed using qPCR on a QuantStudio 6 Flex Real-Time PCR (Applied Biosystems) with TB Green Premix Ex Taq II FAST qPCR (TaKaRa, CN830S) and calculated as % of input. The antibodies against the SP1 (Abcam, ab231778) and RNA polymerase II CTD repeat YSPTSPS (Abcam, ab26721) were used for ChIP assays. All antibodies used were certified as ChIP-grade by the manufacturer. Normal rabbit IgG (Cell Signaling Technology, 2729) was used as a background control. Details of the sequences of the primers are provided in Supplementary Table S1.

Dual-luciferase assays

The MYC promoter containing the promoter elements P1 (including NHE III₁) and P2 was cloned into the pGL3 vector (Promega, Madison, WI) upstream of the firefly luciferase reporter gene. The G4-forming sequence and its variants located upstream of the luciferase reporter gene in the plasmids used in this study are listed in Supplementary Table S1. All fragments inserted into the pGL3 basic vectors were synthesized by Tsingke. The plasmids were purified using the TaKaRa MiniBEST Endo-free Plasmid Purification Kit (Takara, 9783S) and then transfected into 293T cells along with the pRL-TK control reporter vector. Cells were incubated with BTO-28 for 24 h. Relative luciferase activities were measured using the Dual-Luciferase Reporter Assay System (Promega, E1910). Each group was conducted in triplicate.

Results

BTO-28 binds to MYC G4 with high affinity

Quinoline moiety has been shown to stabilize G4 conformations [49, 50], and introduction of positive charges into aliphatic side chain modulates the G4 binding affinity by interfering electrostatic interactions [51]. Our previous studies demonstrated that within the 1-methylquinolinium unit, modification at 2-position could induce the selectivity toward double-stranded DNA (dsDNA) or non-B DNA [52], but the underlying mechanisms governing these distinct recognition abilities remain unclear. In this work, we developed a benzothiazole derivative, BTO-28, which is linked to a 1-methylquinolinium unit, and the functionalization of the molecule with an extra methyl group at 2-position and a cationic side chain aims to modulate its interactions with G4 structures.

Using 1D ¹H NMR spectroscopy, we investigated the interaction between BTO-28 and the MYC G4 under 10 mM K+ conditions. Upon titration of BTO-28 at low concentrations (ratios from 0 to 1), imino protons of MYC G4 were perturbed and a separate set of imino signals emerged (Fig. 1D), which indicates binding interactions. The original imino proton peaks of the free MYC G4 remained visible, suggesting that BTO-28 binds to MYC G4 in a slow-exchange manner on the NMR chemical shift time scale, indicative of highaffinity interactions [53]. Further addition of the molecule induced the appearance of 12 distinct imino proton signals with sharp spectra line widths, indicating the major conformation of BTO-28-MYC G4 complex in solution. Significant perturbations were detected at G15 (in 3' G-tetrad) and G8 (in 5' Gtetrad), while the imino protons of the central G-tetrad exhibited minimal chemical shift changes (Supplementary Fig. S1). These perturbations saturated at concentrations exceeding four molar equivalents of BTO-28. Under 100 mM K⁺ conditions, the NMR titration spectra exhibited a similar binding behavior (Supplementary Fig. S2).

We also visualized BTO-28-bound *MYC* G4 using mass spectrometry [54, 55]. Mass spectrometry analysis at increasing ratios of BTO-28 to *MYC* G4 revealed that the 2:1 complex dominates and that a third binding site is not observed (Supplementary Fig. S3). These findings indicate that BTO-28 interacts mainly with two high-affinity binding sites in *MYC* G4, resulting in a 2:1 stoichiometry. The CD spectra retained characteristics of the parallel folding of *MYC* G4 [56], evidenced by a positive band near 260 nm and a negative band at 240 nm (Supplementary Fig. S4). BTO-28 interacts with high-affinity site of *MYC* G4 with a *K*_D value of 6.8 nM, demonstrating stronger binding than observed for other G4s or dsDNA (Supplementary Fig. S5). These results indicate that BTO-28 binds effectively to the *MYC* G4, with a higher performance compared to other G4 binding compounds [46, 47, 57].

Ligand binding stabilizes G4 structure

Further biophysical analyses were conducted to investigate BTO-28 interaction with MYC G4. Differential scanning calorimetry demonstrated that binding with BTO-28 markedly increased the thermal stability of the G-quadruplex. Specifically, the melting temperatures of MYC G4 rose by 25.6°C for MYC G4 and that of Myc2345 by 26.0°C (Fig. 2A and Supplementary Fig. S6). BTO-28 also significantly enhanced the stability of NHE III₁. In contrast, the molecule destabilized dsDNA, lowering its melting temperature by 4.3°C, likely accounting for its much lower binding affinity toward dsDNA.

The contribution of the high affinity of BTO-28 to G4 stabilization was further investigated by DNA polymerase stop assay. The embedded MYC G4 sequence in the template could form into G4 structure that arrests the polymerase processivity [48, 58]. The mutated sequence that lacks G4-forming ability served as the negative control (Supplementary Table S1). BTO-28 significantly accumulated the truncated products in a concentration-dependent manner, and the full-length extension products became barely appreciable at high BTO-28 concentrations (Fig. 2B). Primer extension using mutated MYC templates indicated that no significant stalling occurred in the presence of the compound (Fig. 2B). These results support that BTO-28 induces G4 formation in the G-rich templates, which impedes DNA synthesis (Fig. 2C).

Comprehensive proton assignment of the 2:1 benzothiazole–*MYC* G4 complex

Oligonucleotides with residue-specifically ¹⁵N-labeled guanines were prepared and then complexed with the molecule. The imino H1 protons were assigned (Supplementary Fig. S7A) by ¹H-¹⁵N HSQC experiments [59] and were further validated by inter-residue NOE correlations. A series of 2D NMR spectra were performed (Fig. 3 and Supplementary Figs S8–S10) to completely assign the nonexchangeable protons and intermolecular NOEs of BTO-28–MYC G4 complex. Each proton showed a single chemical shift (Supplementary Table S2), indicating that BTO-28 binds to the MYC G4 in a single dominant conformation. The characteristic H1–H8 NOEs in G-tetrads combined with the sequential inter-residue H1'-H6/H8 NOE connectivities defined the MYC G4 scaffold (Fig. 3C). Under low ionic strength of 10 mM K⁺, the

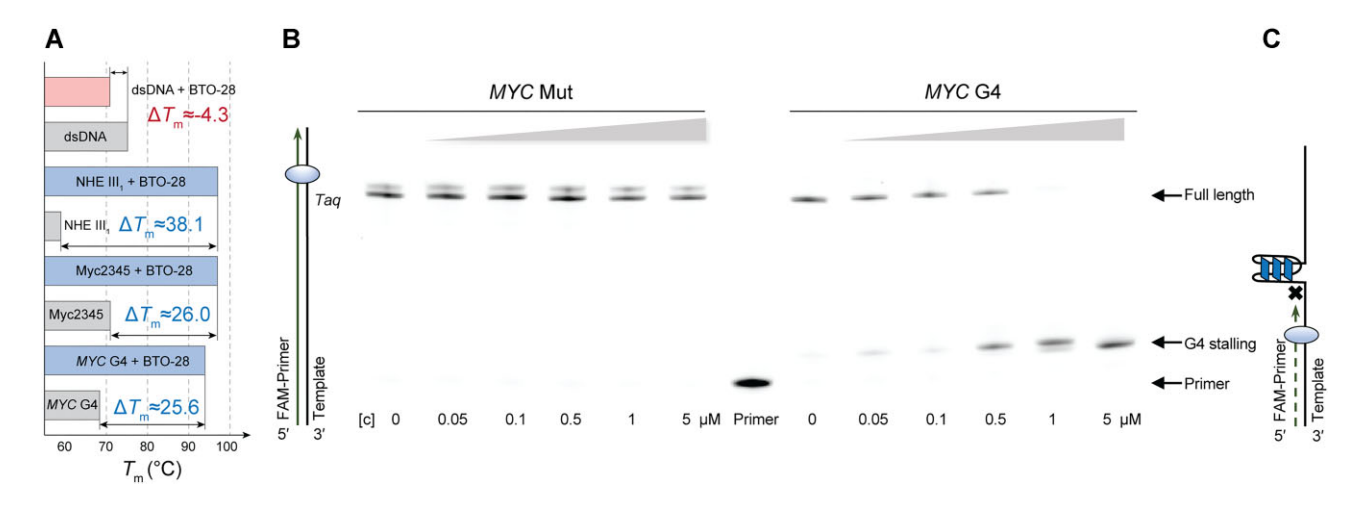


Figure 2. Ligand binding stabilizes MYC G4. (A) DSC melting temperatures of MYC G4, Myc2345, NHE III₁, and dsDNA with or without BTO-28. (B) Taq polymerase stop assays with increasing concentrations of BTO-28 (0.05, 0.1, 0.5, 1, and 5 μ M). The right six panels show the scan for MYC G4, while the left six panels show the scan for MYC G4-mutant. (C) Schematic representation of the polymerase stop assay. The FAM-labeled primer (dark green) is annealed to a G4-forming DNA template (black) and extended by Taq polymerase (light blue).

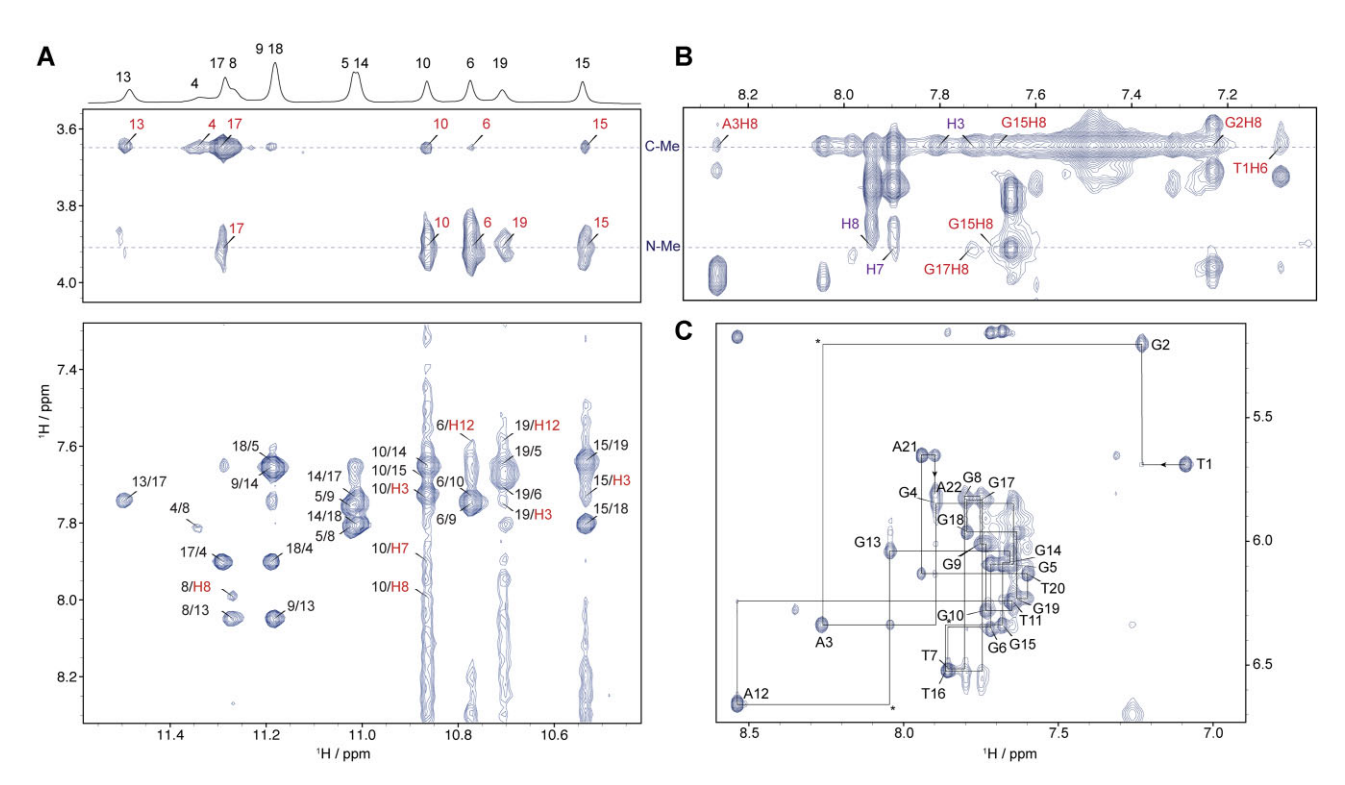


Figure 3. 2D ¹H-¹H NOESY spectra of the 2:1 BTO-28–*MYC* G4 complex. (**A**) Intermolecular NOE cross-peaks (in red) between BTO-28 and *MYC* G4 imino protons. (**B**) Intermolecular NOE contacts between BTO-28 and *MYC* G4 H6/H8 aromatic protons. BTO-28 protons are labeled in red, and intramolecular BTO-28 cross-peaks are labeled in purple. (**C**) Sequential H6–H1′ and H8–H1′ connections (solid lines). Asterisks indicate missing cross-peaks. All spectra were acquired at 298K in 10 mM K⁺ (pH 7.4) with a 300 ms NOESY mixing time.

BTO-28–MYC G4 complex displayed sharper cross-peaks, suggesting that the stronger ligand binding retards the exchange with possible minor conformations. A single set of proton peaks was observed for the 5' and 3'-end overhang residues, suggesting a well-defined stacked conformation at both ends (Supplementary Tables S3 and S4), in contrast to the complicated patterns observed at 100 mM K⁺ (Supplementary Fig. S11). Same complex structures were formed under both conditions, as indicated by the nearly identical resolved regions of the NMR spectra.

From the NOESY spectra, intermolecular NOEs between BTO-28 and MYC G4 protons were identified, and protons of BTO-28 in the bound state were clearly assigned (Supplementary Tables S5–S7). Two sets of methyl signals from BTO-28, labeled C-Me and N-Me, appear at ~3.6 and 3.9 ppm, respectively (Fig. 3A and B). Because these signals are located in a region free from overlapping DNA resonances, multiple intermolecular cross-peaks with tetrad H1 imino protons were clearly assigned. Comparisons of proton chemical shifts between the free and bound states reveal sub-

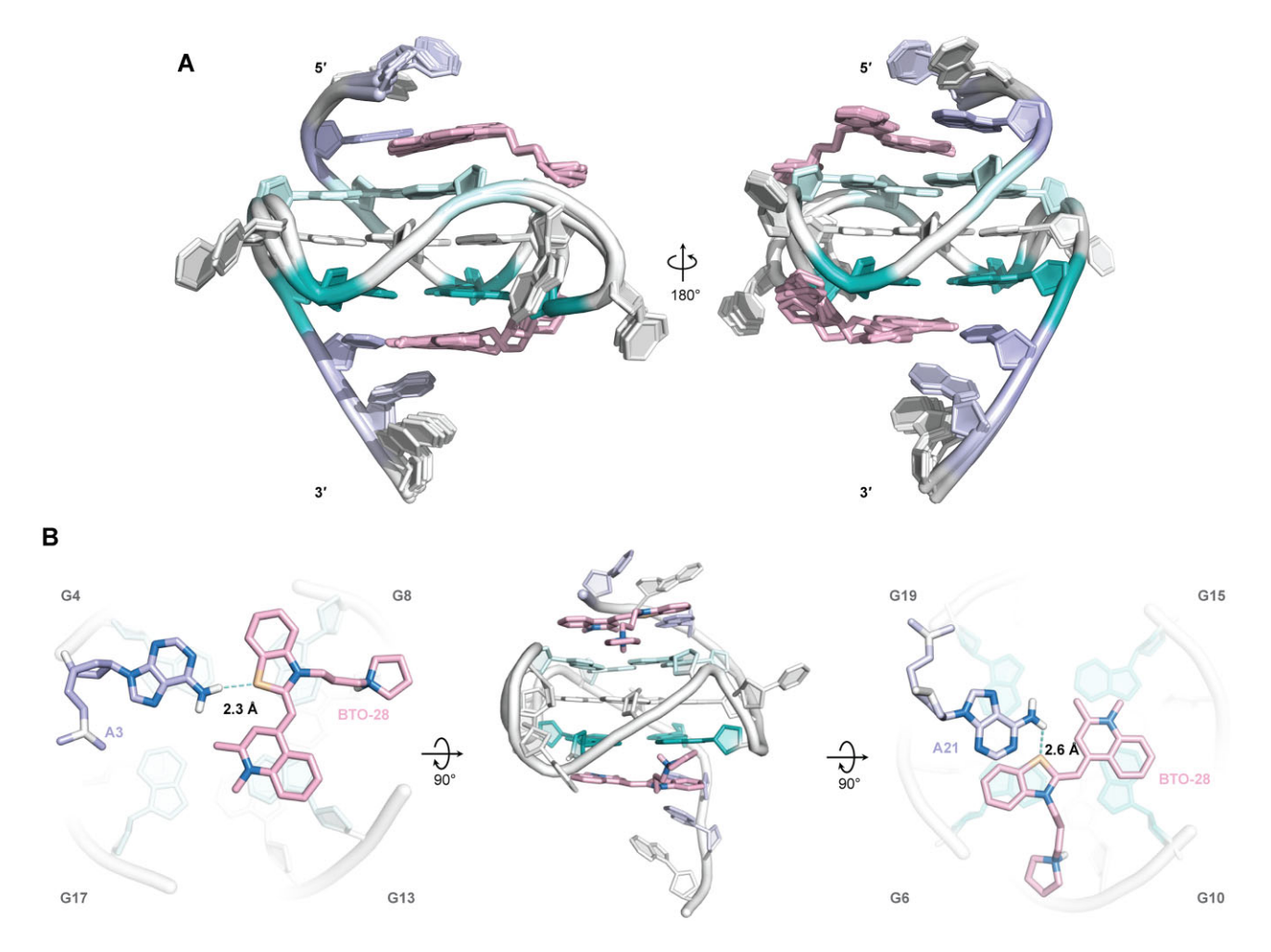


Figure 4. BTO-28–MYC G4 complex reveals additional stacked layers at both termini and flanking-residue rearrangements. (A) Superposition of 10 lowest-energy structures and a representative structure (B) of the 2:1 BTO-28–MYC G4 complex (PDB: 9L4E), shown from the top (left), side (middle), and bottom (right) perspectives. The 5'-tetrad residues are highlighted in pale cyan; the 3'-tetrad residues are in teal; and the flanking residues are in light blue. BTO-28 molecules are depicted in light pink.

stantial conformational rearrangements in both the 5′- and 3′-flanking regions (Supplementary Fig. S1). Loop residues T7 and T16 show only minor chemical shift changes, suggesting they are not part of the primary binding interface.

NMR structure establishes ligand binding mode

Based on NOE-derived intra- and inter-residue distance restraints, along with glycosidic torsion angle and G-tetrad planarity restraints, we employed restrained molecular dynamics to determine the high-resolution structure of the BTO-28-MYC G4 complex. The assembly of the 10 lowest-energy structures showed high convergence, with all heavy atoms root-mean-square deviation (r.m.s.d.) of 0.4 and 0.13 Å for all residues and G-core, respectively (Fig. 4A, PDB ID 9L4E; Table 1). The BTO-28-bound MYC G4 maintains its parallelstranded topology with three propeller loops, yet the flanking regions at both ends rearrange significantly. BTO-28 engages both the 5'- and 3'-end of the MYC G4. The benzothiazole and quinoline rings engage in π - π stacking with the G-tetrads, while its pyrrolidine side chain is accommodated within the groove (Fig. 4B). Compared to the free form, the residue A3 at 5'-end reorients so that its amino group now points toward the central axis (Fig. 5C), as indicated by NOE contacts of A3H2 to G4H1' and BTO-28 H12/H13

Table 1. Structural and NMR statistics for the 2:1 BTO-28-MYC G4 complex

Structure statistics NOE-based distance restraints	
Inter-residue	271
Sequential	184
Long range	30
Medium range	57
BTO-28-G4	102
Deviations from idealized geometry	
Bonds (Å)	0.004 ± 0.000
Angles (°)	0.596 ± 0.004
Impropers (°)	0.364 ± 0.041
NOE violations	
r.m.s.d. of violations	0.043 ± 0.001
Pairwise r.m.s.d. of heavy atoms (Å)	
G-tetrad core	0.13 ± 0.06
All residues	0.45 ± 0.14

protons. This conformation allows the benzothiazole sulfur atom to be involved in hydrogen bonding interaction with the A3 amino group. Earlier investigations on benzoselenazole compounds suggested that this type of interaction is pos-

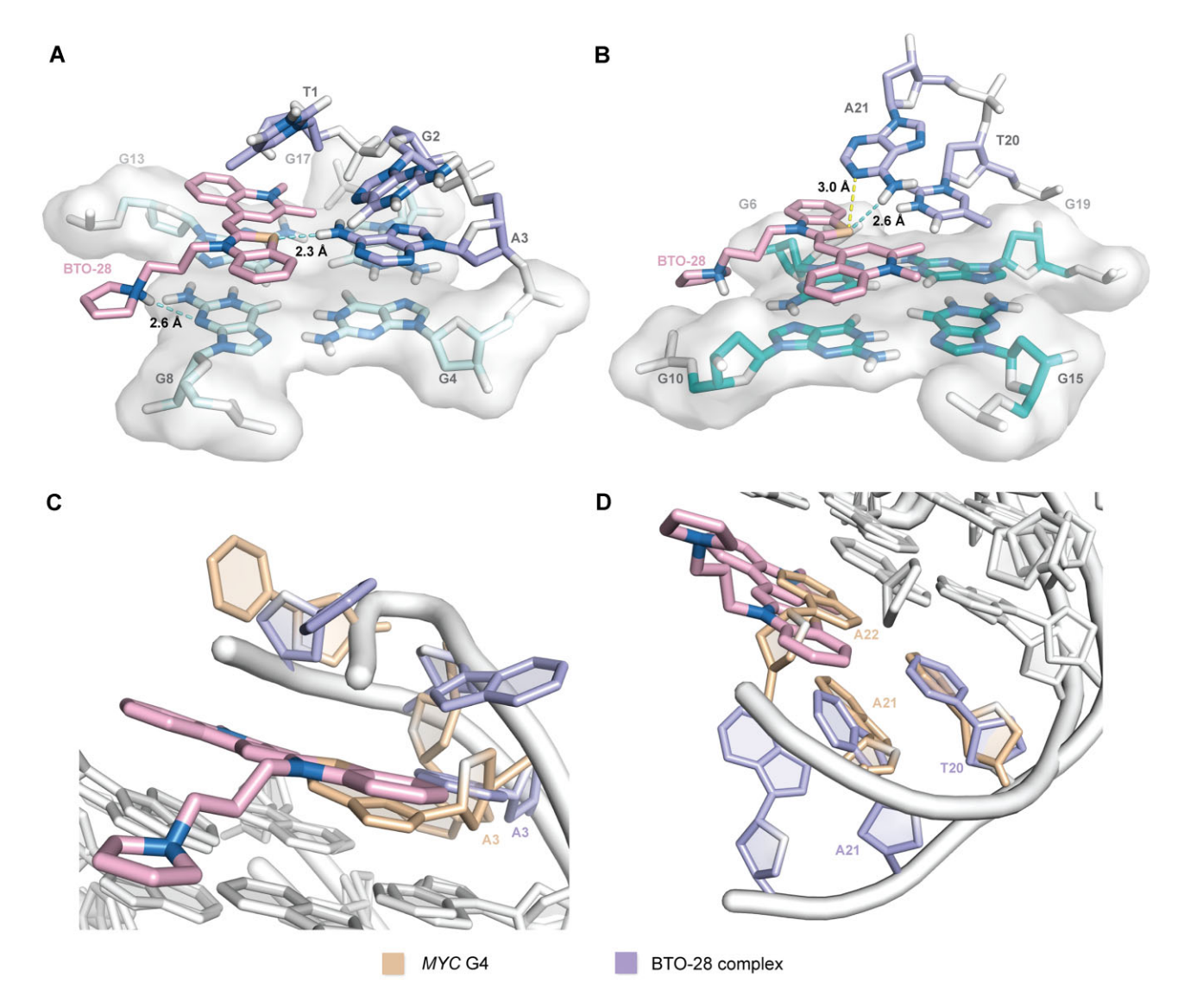


Figure 5. BTO-28 binding explains *MYC* G4 recognition. (A, B) Expanded illustrations of the BTO-28–*MYC* G4 complex at the 5′ (**A**) and 3′ (**B**) ends. Hydrogen bonds are shown as cyan dashed lines, and chalcogen bonds are shown as yellow dashed lines. (C, D) Structural comparisons illustrate conformational differences between the free (PDB: 1XAV) and BTO-28–bound *MYC* G4 at the 5′ (**C**) and 3′ (**D**) ends. Superimposed structures highlight reorientation of the flanking residues, each color-coded as indicated.

sible [57]. The well-stacked position of A3 was also supported by the profound downfield shifting of its H2 and H8 protons and an upfield shifting in G4H1 (Supplementary Fig. S1). Meanwhile, T1 and G2 reposition to stack over the BTO-28-adenine plane. Under these conditions, BTO-28 adopts a more planar conformation that aligns with the external tetrad, covering G8 and G13 (Fig. 5A). Intermolecular NOEs connecting G8 imino protons to the BTO-28 benzothiazole moiety and G13 imino protons to the BTO-28 quinoline moiety indicate that BTO-28 is anchored in a defined conformation (Supplementary Fig. S12A). Additionally, intermolecular NOEs involving both BTO-28 methyl groups and G17H1 protons were also observed, and intramolecular NOEs involving BTO-28 H3/H12 and H5/H9 protons provided supplementary validation of these ligand-induced conformational states. The presence of adjacent bases in the binding pocket might stabilize the coplanar immobilization of the benzothiazole and quinolinium groups [60-62], consistent with the fluorescence enhancement upon binding to G-quadruplex [63].

At the 3'-end, the initial stacking mode of A21 over the T20-A22 base pairing is disrupted, and instead, T20 integrates into the BTO-28-base plane stacking on the 3'-tetrad (Fig. 5B). NOE connections linking A21H2 to the benzothiazole aromatic protons further confirm the new capping conformation of the 3'-overhang residues, which ultimately forms a new binding pocket (Fig. 5D). This arrangement enables a hydrogen bond between the A21 NH₂ group and the BTO-28 benzothiazole sulfur atom. Numerous NOE cross-peaks between the BTO-28 aromatic protons and G6H1/H8 as well as G10H1/H8 revealed clearly defined orientations of the benzothiazole molecule (Supplementary Fig. S12B). Two methyl groups within the quinoline unit point to the emptier region adjacent to the groove bordered by G15 to G19. This is supported by medium-intensity NOE cross-peaks involving all the imino protons of the 3'-tetrad and the N-Me group. Alter-

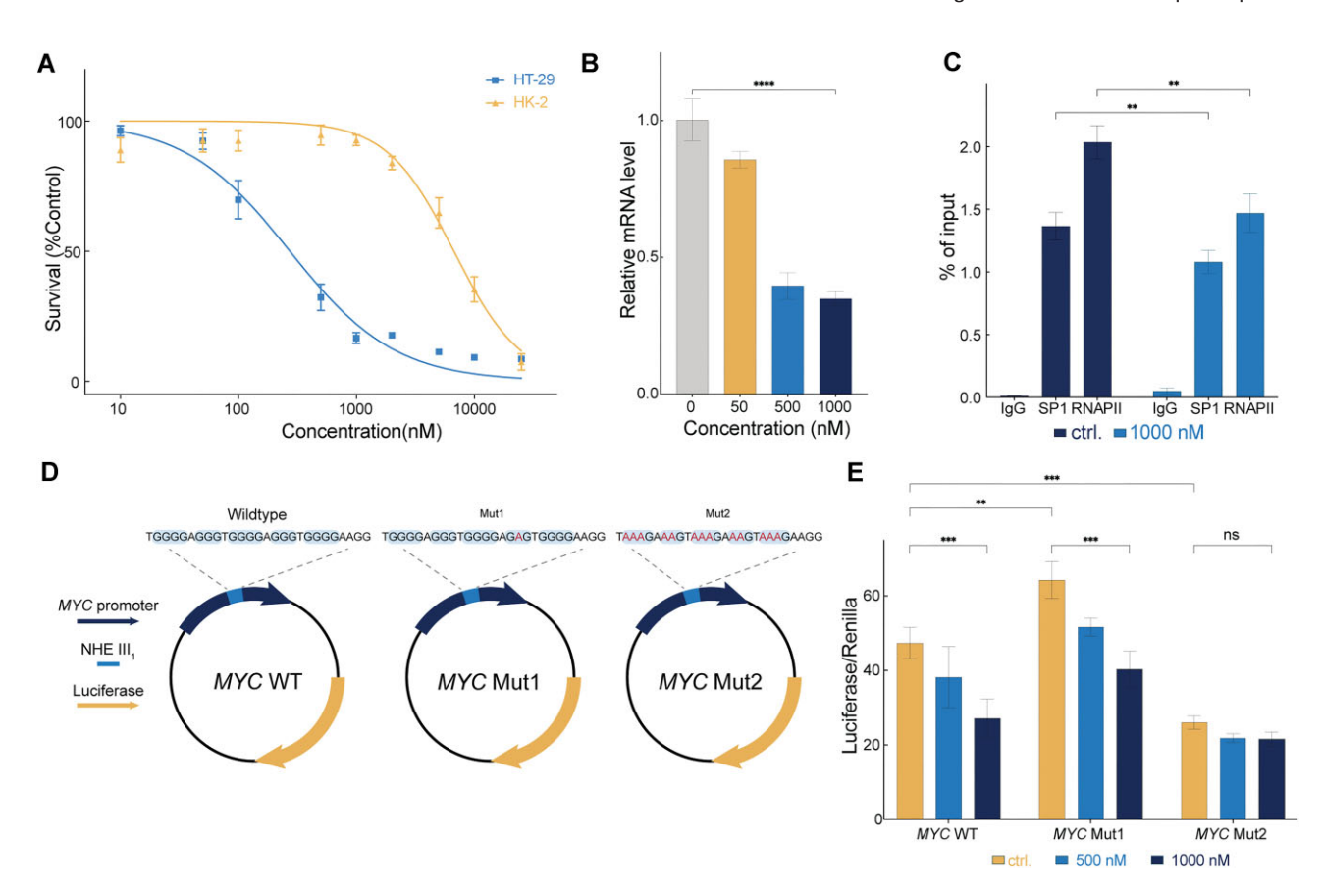


Figure 6. BTO-28 regulates MYC transcription. (A) Effects of compounds on the proliferation of different cell lines. Data represent the mean of three independent experiments. (B) Quantification of MYC mRNA in HT-29 cells treated with the quantified BTO-28 compounds. All mRNA levels are normalized to β-actin, and the $\Delta\Delta C_t$ method was employed for relative gene expression analysis. Error bars represent the standard deviation from three biological replicates. ****P < .0001. (C) ChIP of the interaction between SP1 and the MYC promoter shows that BTO-28 disrupts SP1 binding to the G4-forming region of the MYC promoter. n = 4 biologically independent samples. Error bars represent the mean ± standard deviation (SD). Statistical significance was determined using Bonferroni's multiple comparisons test following a two-way ANOVA. **P < .01. (D) Schematic diagram of plasmids containing NHE III₁ region and its variants cloned upstream of the luciferase reporter gene. (E) Relative luciferase expression by the MYC promoters normalized to the renilla plasmid after treatment with BTO-28. Error bars represent the mean ± SD (n = 3). t test. ns, nonsignificant difference; **P < .01: ***P < .001.

natively, the 3'-terminal A22 conformations remain flexible, exhibiting few NOE interactions.

The side chain of BTO-28 plays a considerable role in facilitating specific interactions with MYC G4. Although the protonated HN3 could not be observed due to rapid solvent exchange, intermolecular NOE connections between the benzothiazole H6' protons and G8H21/H1' demonstrate that the pyrrolidine side chain accommodates into the groove bordered by G8 to G13. Additionally, a potential hydrogen bond is formed between G8N3 and HN3 with a distance of ~2.6 Å (Fig. 5A), with the N3 nitrogen of guanine as the acceptor [64]. Lower salt concentration might strengthen this hydrogen bond [65], which may account for the higher benzothiazole binding observed at the 5' end. At the 3'-terminal, similar NOE pattern was observed between the BTO-28 side chain and G6. However, the protonated HN3 does not exhibit a close spatial proximity to G6N3, suggesting a weaker yet plausible hydrogen bonding interaction. The flexibility of residue T7 along with the hydrogen bond between A21 and benzothiazole likely limits the ligand-groove interaction. This effect may also explain the stronger affinity observed for the MYC G4 at 5' end. Collectively, NMR structure establishes a binding mode in which one BTO-28 molecule covers the top G-tetrad, while another covers the bottom G-tetrad.

We also conducted 1D ¹H NMR titration and ¹H-¹⁵N-HSQC experiments of BTO-28 with the Myc2345 sequence [40]. Myc2345 contains the conserved guanine at position 20 in the 3'-flanking sequence, where MYC G4 includes a G-to-T mutation to reduce the conformational polymorphism [37]. The resemblance of the imino proton resonances in the 2:1 BTO-28 complexed with MYC G4 and Myc2345 indicates that both sequences share a similar G-quadruplex topology (Supplementary Fig. S7), which is consistent with the same binding pattern observed in mass spectrometry (Supplementary Figs S3 and S13).

BTO-28 regulates MYC transcription

Cell viability assays revealed that BTO-28 effectively inhibited the proliferation of colorectal carcinoma (HT-29) cells, with IC₅₀ values of ~273 nM, indicating a higher level of activity compared to other G4 ligands [39, 66]. Notably, it did not inhibit the growth of normal kidney cells (HK-2) at concentrations up to 5 μ M (Fig. 6A). Given that proto-oncogenes such as MYC, KRAS, RET, and VEGF are often overexpressed in human cancers, we analyzed the regulatory effect of BTO-28 on proto-oncogene transcription in HT-29 cells. MYC downregulation mediated by G4 stabilization was

measured using P1-promoter primers [28, 30]. Downregulation of P1-driven MYC expression was observed with BTO-28 (Fig. 6B). In contrast, treatment with BTO-28 did not cause a concentration-dependent decrease in the expression of *RET*, *bTERT*, *KIT*, *KRAS*, and *VEGF* in HT-29 cells compared to controls (Supplementary Fig. S14).

To determine whether the reduced MYC transcription caused by BTO-28 is related to the inhibition of SP1 binding to the MYC promoter, we performed ChIP analysis on HT-29 cells. Treatment with BTO-28 resulted in a decrease in SP1 occupancy at the MYC promoter (Fig. 6C). The formation of G4-DNA structures may impede the transcription elongation by RNA polymerase II (RNAPII), thereby inhibiting gene expression [67]. Aligned with this, cells treated with BTO-28 showed reductions in RNAPII binding at the MYC promoter. Collectively, these results indicate that BTO-28 may disrupt the interaction between these transcription factors and the MYC promoter G4.

Dual-luciferase assay has been used to examine the effect of G4 formation in NHE III₁ on gene transcription. The MYC promoter that contains NHE III₁ and the two major promoter regions, P1 and P2, was cloned into the pGL3 vector upstream of the firefly luciferase reporter gene to obtain the construct MYC WT [68]. An earlier study demonstrated that the MYC Mut1 construct, which contains a single G-to-A substitution that destabilizes the G4 motif, resulted in a significant increase in transcriptional activation compared to that of the wild-type NHE III₁ sequence [6]. The primary G-quadruplex structure within the NHE III₁ region responsible for MYC transcription silencing involves four consecutive G-runs at the 3'-end [48]. A second mutant in which all core guanines involved in G4 scaffold were replaced by adenines was constructed to completely obstruct G4 formation (Fig. 6D). Compared to the wild-type promoter, introducing a single-base mutation enhanced promoter activity in cells. While the promoter activity of MYC Mut2, which contains multiple point mutations sufficient to prevent G-quadruplex formation, was diminished (Fig. 6E), this reduction suggests that NHE III₁ with core guanine substitutions may impede transcription complexes or inhibit the binding of positive transcription factors, leading to decreased transcription levels [69].

BTO-28 significantly reduced the luciferase activity of the reporter construct containing wild-type MYC compared to the control. Although the single-base mutant exhibited enhanced promoter activity compared to the wild type, modest reductions were observed at high drug concentrations. This suggests that the stabilizing effects of BTO-28 can partially counteract the destabilizing impact of the single-base mutation. Intriguingly, BTO-28 did not inhibit the luciferase expression of MYC Mut2 (Fig. 6E). These results suggest that BTO-28 likely inhibits MYC transcription by influencing specific G-quadruplex structure within the NHE III₁ region.

Discussion

Comprehensive NMR structural studies of BTO-28 in complex with MYC G4 offer precise insights into the molecular interactions driving G-quadruplex recognition. Systematic structural analyses of various ligand complexes uncovered a shared binding mode: small, arc-shaped molecules feature a broad planar surface for π - π stacking on the external G-tetrads [37, 40]. They also engage flexible flanking residues at both 5' and 3' ends, adapting their conformation to maintain

stable binding [70]. Hydrogen bonding involving the recruited residue is scarce in previously characterized complexes and has only been observed at the 3'-end for quindoline [65] and DC-34 [71] bound to the MYC G4. Here, for the first time, we describe a unique hydrogen-bonding pattern between a nucle-obase surrogate and the flanking bases. The sulfur in the benzothiazole core forms hydrogen bonds with the NH₂ groups of A3 and A21, respectively, and engages in chalcogen bonds with adenine N1 atom. BTO-28 might interfere with canonical base pairing in dsDNA, leading to decreased stability. Conversely, upon binding to MYC G4, the molecule utilizes a base recruitment mechanism to reinforce the structure through hydrogen bonding and stacking interactions. Through these interactions with the G4, BTO-28 establishes a distinct binding mode not observed for previously reported ligands.

Incorporating positive charges into attached side chains is a commonly used strategy for promoting G4 binding, primarily by leveraging electrostatic interactions [51]. In quindoline derivatives, for instance, the diethylamino group resides 2.7 Å from the DNA phosphate backbone, whereas the azepane ring in DC-34 is too short and bulky to support such an interaction (Supplementary Fig. S15) [71]. By contrast, the optimal number of carbon atoms linking the benzothiazole core to the amine in BTO-28, combined with the appropriate steric hindrance of the flexible pyrrolidine, facilitates hydrogen bonding with the 5' external G-tetrad and electrostatic engagement within G4 grooves. Such interactions appear to stabilize and properly orient the benzothiazole, which may underlie the observed comparative specificity in chemical and biological assays. No interaction has been documented previously between positively charged side chains and the external G-tetrads, highlighting the importance of refining ligand-G4 interface within the groove dimensions. Changing the pyrrolidine ring to other aliphatic amines led to small decreases in potency, whereas attempts with morpholine heterocycles yielded uniformly inferior results. In parallel, altering the 2position methyl on 1-methylquinolinium to styryl moieties significantly reduced activity (Supplementary Fig. S16). Subtle adjustments to the shape and electrostatic properties of the ligand will influence its precise orientation within the intercalated pockets. Benzothiazole binding at the 5'-flanking region is driven strongly by specific residue interactions, whereas 3'-end binding appears more dependent on the surrounding ionic environment. These variations reflect inherent structural differences: the 5'-terminal is more hydrophobic, promoting reduced solvent exposure and strengthened hydrogen bonds [72], while the 3'-terminal remains relatively hydrophilic and less favorable for ligand stacking. This contrast explains the stronger binding affinity measured at the 5' end. It is also worth noting that the wild-type Myc2345 sequence appears to adopt the same conformation in the 2:1 benzothiazole complex.

Our research targeted the recognition of the G4 element within the human MYC NHE III₁ locus. Multiple independent assays demonstrated that BTO-28 stabilizes the G4 structure and promotes the refolding of DNA flanking regions. These results present a potentially mechanism of MYC transcriptional inhibition via G4 targeting. While BTO-28 shows strong binding to MYC G4, the widespread presence of G4 motifs across the genome may lead to the risk of off-target effects by engaging unrelated G4 structures in other mammalian genes. We envision that integrating BTO-28 with recently developed ATENA (Approach to Target Exact Nucleic Acid al-

ternative structures) will enable precise targeting for MYC G4 [30], thereby minimizing unintended interactions with non-relevant G4s.

Conclusions

Overall, our study of the interaction between MYC G-quadruplex and BTO-28 provides valuable insights into how ligand-induced structural changes in G4 DNA may orchestrate complex transcriptional processes. BTO-28 exhibits unique binding at the 5'- and 3'-termini of the MYC G4. By uncovering base sequences critical for low nanomolar affinity, we highlight that stacking interactions and groove interactions together enable G4 targeting. Also, our study indicates that G-quadruplex formation is intricately linked to MYC gene expression. These findings provide an important rationale for end-specific interactions of BTO-28 in shaping MYC G4 stability and functionality.

Acknowledgements

We thank the staff members of the Nuclear Magnetic Resonance System (https://cstr.cn/31129.02.NFPS.NMRSystem) at the National Facility for Protein Science in Shanghai (https://cstr.cn/31129.02.NFPS), Shanghai Advanced Research Institute, Chinese Academy of Sciences (CAS), Steady High Magnetic Field Facilities, High-Field Magnetic Laboratory (HFML), CAS, Hefei, Anhui Province, and NMR center of Shanghai Institute of Materia Medica (SIMM), CAS, for providing technical support and assistance in data collection and analysis. The University Research Facilities on Life Sciences of the Hong Kong Polytechnic University is also acknowledged.

Author contributions: Xiao NI: conceptualization, investigation, formal analysis, methodology, validation, visualization, writing—original draft. Xiao-Dong Hu: investigation, formal analysis. Wei Long: investigation, formal analysis. Wenxian Lan: methodology, formal analysis. Chunxi Wang: methodology, formal analysis. Wing-Leung Wong: project administration, supervision. Chunyang Cao: conceptualization, formal analysis, funding acquisition, project administration, supervision, writing—review & editing.

Supplementary data

Supplementary data is available at NAR online.

Conflict of interest

None declared.

Funding

This work was funded by the Strategic Priority Research Program of the Chinese Academy of Sciences (Grant No. XDB1060000), National Natural Science Foundation of China (NSFC) (22177127 and 22174155), and the Research Grants Council of the Hong Kong Special Administrative Region, China (RGC Project No. 15300522). W.L. acknowledges the award of a postdoctoral fellowship administered by the Research Committee of the Hong Kong Polytechnic University. Funding to pay the Open Access publication charges for this article was provided by the Strategic Priority Research

Program of the Chinese Academy of Sciences (Grant No. XDB1060000).

Data availability

The coordinates for structures of the 2:1 BTO-28–MYC G4 complex (PDB code: 9L4E) have been deposited in the Protein Data Bank. Chemical shift assignments were also deposited in BMRB with accession code 36722.

References

- 1. Monsen RC, DeLeeuw LW, Dean WL *et al.* Long promoter sequences form higher-order G-quadruplexes: an integrative structural biology study of *c-Myc*, *k-Ras* and *c-Kit* promoter sequences. *Nucleic Acids Res* 2022;50:4127–47. https://doi.org/10.1093/nar/gkac182
- Zhang X, Spiegel J, Martínez Cuesta S et al. Chemical profiling of DNA G-quadruplex-interacting proteins in live cells. Nat Chem 2021;13:626–33. https://doi.org/10.1038/s41557-021-00736-9
- 3. Di Antonio M, Ponjavic A, Radzevičius A *et al.* Single-molecule visualization of DNA G-quadruplex formation in live cells. *Nat Chem* 2020;12:832–7. https://doi.org/10.1038/s41557-020-0506-4
- 4. Jansson LI, Hentschel J, Parks JW *et al.* Telomere DNA G-quadruplex folding within actively extending human telomerase. *Proc Natl Acad Sci USA* 2019;**116**:9350–9. https://doi.org/10.1073/pnas.1814777116
- 5. Phan AT, Kuryavyi V, Gaw HY *et al.* Small-molecule interaction with a five-guanine-tract G-quadruplex structure from the human MYC promoter. *Nat Chem Biol* 2005;1:167–73. https://doi.org/10.1038/nchembio723
- Siddiqui-Jain A, Grand CL, Bearss DJ et al. Direct evidence for a G-quadruplex in a promoter region and its targeting with a small molecule to repress c-MYC transcription. Proc Natl Acad Sci USA 2002;99:11593–8. https://doi.org/10.1073/pnas.182256799
- 7. Liu Y, Li J, Zhang Y *et al.* Structure of the major G-quadruplex in the human *EGFR* oncogene promoter adopts a unique folding topology with a distinctive snap-back loop. *J Am Chem Soc* 2023;145:16228–37. https://doi.org/10.1021/jacs.3c05214
- 8. Ducani C, Bernardinelli G, Högberg B *et al.* Interplay of three G-quadruplex units in the KIT promoter. *J Am Chem Soc* 2019;141:10205–13. https://doi.org/10.1021/jacs.8b12753
- Lee C-Y, Joshi M, Wang A et al. 5'UTR G-quadruplex structure enhances translation in size dependent manner. Nat Commun 2024;15:3963. https://doi.org/10.1038/s41467-024-48247-8
- Li C, Wang H, Yin Z et al. Ligand-induced native G-quadruplex stabilization impairs transcription initiation. Genome Res 2021;31:1546–60. https://doi.org/10.1101/gr.275431.121
- Yu Z, Spiegel J, Melidis L et al. Chem-map profiles drug binding to chromatin in cells. Nat Biotechnol 2023;41:1265–71. https://doi.org/10.1038/s41587-022-01636-0
- 12. Wang G, Vasquez KM. Dynamic alternative DNA structures in biology and disease. *Nat Rev Genet* 2023;24:211–34. https://doi.org/10.1038/s41576-022-00539-9
- Llombart V, Mansour MR. Therapeutic targeting of "undruggable" MYC. eBiomedicine 2022;75:103756. https://doi.org/10.1016/j.ebiom.2021.103756
- Harrington CT, Sotillo E, Dang CV et al. Tilting MYC toward cancer cell death. Trends Cancer 2021;7:982–94. https://doi.org/10.1016/j.trecan.2021.08.002
- Jakobsen ST, Jensen RAM, Madsen MS et al. MYC activity at enhancers drives prognostic transcriptional programs through an epigenetic switch. Nat Genet 2024;56:663–74. https://doi.org/10.1038/s41588-024-01676-z
- Dang CV, Reddy EP, Shokat KM et al. Drugging the 'undruggable' cancer targets. Nat Rev Cancer 2017;17:502–8. https://doi.org/10.1038/nrc.2017.36

- 17. Dhanasekaran R, Deutzmann A, Mahauad-Fernandez WD *et al*. The MYC oncogene—the grand orchestrator of cancer growth and immune evasion. *Nat Rev Clin Oncol* 2022;19:23–36. https://doi.org/10.1038/s41571-021-00549-2
- Whitfield JR, Soucek L. MYC in cancer: from undruggable target to clinical trials. Nat Rev Drug Discov 2025;24:445–57. https://doi.org/10.1038/s41573-025-01143-2
- Lourenco C, Resetca D, Redel C et al. MYC protein interactors in gene transcription and cancer. Nat Rev Cancer 2021;21:579–91. https://doi.org/10.1038/s41568-021-00367-9
- 20. Holmes AG, Parker JB, Sagar V et al. A MYC inhibitor selectively alters the MYC and MAX cistromes and modulates the epigenomic landscape to regulate target gene expression. Sci Adv 2022;8:eabh3635. https://doi.org/10.1126/sciadv.abh3635
- Garralda E, Beaulieu M-E, Moreno V et al. MYC targeting by OMO-103 in solid tumors: a phase 1 trial. Nat Med 2024;30:762–71. https://doi.org/10.1038/s41591-024-02805-1
- Karadkhelkar NM, Lin M, Eubanks LM et al. Demystifying the druggability of the MYC family of oncogenes. J Am Chem Soc 2023;145:3259–69. https://doi.org/10.1021/jacs.2c12732
- Selvam S, Koirala D, Yu Z. et al. Quantification of topological coupling between DNA superhelicity and G-quadruplex formation. J Am Chem Soc 2014;136:13967–70. https://doi.org/10.1021/ja5064394
- Brooks TA, Hurley LH. The role of supercoiling in transcriptional control of MYC and its importance in molecular therapeutics. *Nat Rev Cancer* 2009;9:849–61. https://doi.org/10.1038/nrc2733
- Brooks TA, Hurley LH. Targeting MYC Expression through G-Quadruplexes. Genes Cancer 2010;1:641–9. https://doi.org/10.1177/1947601910377493
- González V, Hurley LH. The c-MYC NHE III(1): function and regulation. Annu Rev Pharmacol Toxicol 2010;50:111–29. https://doi.org/10.1146/annurev.pharmtox.48.113006.094649
- Chen L, Dickerhoff J, Zheng K-w et al. Structural basis for nucleolin recognition of MYC promoter G-quadruplex. Science 2025;388:eadr1752. https://doi.org/10.1126/science.adr1752
- 28. Esain-Garcia I, Kirchner A, Melidis L *et al*. G-quadruplex DNA structure is a positive regulator of *MYC* transcription. *Proc Natl Acad Sci USA* 2024;121:e2320240121. https://doi.org/10.1073/pnas.2320240121
- 29. Galli S, Melidis L, Flynn SM *et al.* DNA G-quadruplex recognition *in vitro* and in live cells by a structure-specific nanobody. *J Am Chem Soc* 2022;144:23096–103. https://doi.org/10.1021/jacs.2c10656
- 30. Nuccio SP, Cadoni E, Nikoloudaki R. et al. Chemically modified CRISPR-Cas9 enables targeting of individual G-quadruplex and i-motif structures, revealing ligand-dependent transcriptional perturbation. bioRxiv, https://doi.org/10.1101/2024.10.14.618195, 22 July 2025, preprint: not peer reviewed.
- 31. Sun H, Sun R, Yang D *et al.* A cyanine dye for highly specific recognition of parallel G-quadruplex topology and its application in clinical RNA detection for cancer diagnosis. *J Am Chem Soc* 2024;146:22736–46. https://doi.org/10.1021/jacs.4c07698
- 32. Zhang X, Dhir S, Melidis L *et al.* Optical control of gene expression using a DNA G-quadruplex targeting reversible photoswitch. *Nat Chem* 2025;17:875–82. https://doi.org/10.1038/s41557-025-01792-1
- 33. Koh GCC, Boushaki S, Zhao SJ *et al.* The chemotherapeutic drug CX-5461 is a potent mutagen in cultured human cells. *Nat Genet* 2024;56:23–6. https://doi.org/10.1038/s41588-023-01602-9
- 34. Hilton J, Gelmon K, Bedard PL et al. Results of the phase I CCTG IND.231 trial of CX-5461 in patients with advanced solid tumors enriched for DNA-repair deficiencies. Nat Commun 2022;13:3607. https://doi.org/10.1038/s41467-022-31199-2
- 35. Pan M, Wright WC, Chapple RH et al. The chemotherapeutic CX-5461 primarily targets TOP2B and exhibits selective activity in high-risk neuroblastoma. Nat Commun 2021;12:6468. https://doi.org/10.1038/s41467-021-26640-x

- Varshney D, Spiegel J, Zyner K et al. The regulation and functions of DNA and RNA G-quadruplexes. Nat Rev Mol Cell Biol 2020;21:459–74. https://doi.org/10.1038/s41580-020-0236-x
- Ambrus A, Chen D, Dai J et al. Solution structure of the biologically relevant G-quadruplex element in the human c-MYC promoter. Implications for G-quadruplex stabilization. Biochemistry 2005;44:2048–58. https://doi.org/10.1021/bi048242p
- 38. Stump S, Mou T-C, Sprang SR *et al.* Crystal structure of the major quadruplex formed in the promoter region of the human c-MYC oncogene. *PLoS One* 2018;13:e0205584. https://doi.org/10.1371/journal.pone.0205584
- 39. Liu W, Zhu B-C, Liu L-Y *et al.* Solution structures and effects of a platinum compound successively bound MYC G-quadruplex. *Nucleic Acids Res* 2024;52:9397–406. https://doi.org/10.1093/nar/gkae649
- Dickerhoff J, Dai J, Yang D. Structural recognition of the MYC promoter G-quadruplex by a quinoline derivative: insights into molecular targeting of parallel G-quadruplexes. *Nucleic Acids Res* 2021;49:5905–15. https://doi.org/10.1093/nar/gkab330
- Okamoto A. ECHO probes: a concept of fluorescence control for practical nucleic acid sensing. *Chem Soc Rev* 2011;40:5815–28. https://doi.org/10.1039/c1cs15025a
- **42.** Sato T, Sato Y, Nishizawa S. Triplex-forming peptide nucleic acid probe having thiazole orange as a base surrogate for fluorescence sensing of double-stranded RNA. *J Am Chem Soc* 2016;138:9397–400. https://doi.org/10.1021/jacs.6b05554
- 43. Silva GL, Ediz V, Yaron D et al. Experimental and computational investigation of unsymmetrical cyanine dyes: understanding torsionally responsive fluorogenic dyes. J Am Chem Soc 2007;129:5710–8. https://doi.org/10.1021/ja070025z
- 44. Nazarenko I, Pires R, Lowe B et al. Effect of primary and secondary structure of oligodeoxyribonucleotides on the fluorescent properties of conjugated dyes. Nucleic Acids Res 2002;30:2089–195. https://doi.org/10.1093/nar/30.9.2089
- 45. Long W, Zeng Y-X, Zheng B-X et al. Targeting hTERT promoter G-quadruplex DNA structures with small-molecule ligand to downregulate hTERT expression for triple-negative breast cancer therapy. J Med Chem 2024;67:13363–82. https://doi.org/10.1021/acs.jmedchem.4c01255
- 46. Long W, Zheng B-X, Li Y et al. Rational design of small-molecules to recognize G-quadruplexes of c-MYC promoter and telomere and the evaluation of their in vivo antitumor activity against breast cancer. Nucleic Acids Res 2022;50:1829–48. https://doi.org/10.1093/nar/gkac090
- 47. Wang F, Wang C, Liu Y et al. Colchicine selective interaction with oncogene RET G-quadruplex revealed by NMR. Chem Commun 2020;56:2099–102. https://doi.org/10.1039/D0CC00221F
- Seenisamy J, Rezler EM, Powell TJ et al. The dynamic character of the G-quadruplex element in the c-MYC promoter and modification by TMPyP4. J Am Chem Soc 2004;126:8702–9. https://doi.org/10.1021/ja040022b
- 49. Liu L-Y, Ma T-Z, Zeng Y-L *et al.* Structural basis of pyridostatin and its derivatives specifically binding to G-quadruplexes. *J Am Chem Soc* 2022;144:11878–87. https://doi.org/10.1021/jacs.2c04775
- 50. Ghosh A, Trajkovski M, Teulade-Fichou M-P et al. Phen-DC3 induces refolding of human telomeric DNA into a chair-type antiparallel G-quadruplex through ligand intercalation. Angew Chem Int Ed Engl 2022;61:e202207384. https://doi.org/10.1002/anie.202207384
- 51. Chung WJ, Heddi B, Tera M et al. Solution structure of an intramolecular (3 + 1) human telomeric G-quadruplex bound to a telomestatin derivative. J Am Chem Soc 2013;135:13495–501. https://doi.org/10.1021/ja405843r
- 52. Lu Y-J, Deng Q, Hou J-Q et al. Molecular engineering of thiazole orange dye: change of fluorescent signaling from universal to specific upon binding with nucleic acids in bioassay. ACS Chem

- *Biol* 2016;11:1019–29. https://doi.org/10.1021/acschembio.5b00987
- 53. Zimmermann GR, Jenison RD, Wick CL et al. Interlocking structural motifs mediate molecular discrimination by a theophylline-binding RNA. Nat Struct Mol Biol 1997;4:644–9. https://doi.org/10.1038/nsb0897-644
- 54. Ghosh A, Largy E, Gabelica V. DNA G-quadruplexes for native mass spectrometry in potassium: a database of validated structures in electrospray-compatible conditions. *Nucleic Acids Res* 2021;49:2333–45. https://doi.org/10.1093/nar/gkab039
- Largy E, König A, Ghosh A et al. Mass spectrometry of nucleic acid noncovalent complexes. Chem Rev 2022;122:7720–839. https://doi.org/10.1021/acs.chemrev.1c00386
- 56. Karsisiotis AI, Hessari NMa, Novellino E et al. Topological characterization of nucleic acid G-quadruplexes by UV absorption and circular dichroism. Angew Chem Int Ed Engl 2011;50:10645–8. https://doi.org/10.1002/anie.201105193
- 57. Wu T-Y, Chen X-C, Tang G-X et al. Development and characterization of benzoselenazole derivatives as potent and selective c-MYC transcription inhibitors. J Med Chem 2023;66:5484–99. https://doi.org/10.1021/acs.jmedchem.2c01808
- Han H, Hurley LH, Salazar M. A DNA polymerase stop assay for G-quadruplex-interactive compounds. *Nucleic Acids Res* 1999;27:537–42. https://doi.org/10.1093/nar/27.2.537
- 59. Dai J, Dexheimer TS, Chen D et al. An intramolecular G-quadruplex structure with mixed parallel/antiparallel G-strands formed in the human BCL-2 promoter region in solution. J Am Chem Soc 2006;128:1096–8. https://doi.org/10.1021/ja055636a
- 60. Hannah KC, Armitage BA. DNA-templated assembly of helical cyanine dye aggregates: a supramolecular chain polymerization. *Acc Chem Res* 2004;37:845–53. https://doi.org/10.1021/ar030257c
- 61. Karunakaran V, Pérez Lustres JL, Zhao L *et al.* Large dynamic stokes shift of DNA intercalation dye thiazole orange has contribution from a high-frequency mode. *J Am Chem Soc* 2006;128:2954–62. https://doi.org/10.1021/ja056862n
- 62. Yang P, De Cian A, Teulade-Fichou MP et al. Engineering bisquinolinium/thiazole orange conjugates for fluorescent sensing of G-quadruplex DNA. Angew Chem Int Ed Engl 2009;48:2188–91. https://doi.org/10.1002/anie.200805613

- 63. Long W, Lu Y-J, Zhang K *et al.* Boosting the turn-on fluorescent signaling ability of thiazole orange dyes: the effectiveness of structural modification site and its unusual interaction behavior with nucleic acids. *Dyes Pigm* 2018;159:449–56. https://doi.org/10.1016/j.dyepig.2018.07.008
- 64. Noeske J, Richter C, Grundl MA et al. An intermolecular base triple as the basis of ligand specificity and affinity in the guanineand adenine-sensing riboswitch RNAs. Proc Natl Acad Sci USA 2005;102:1372–7. https://doi.org/10.1073/pnas.0406347102
- 65. Dai J, Carver M, Hurley LH et al. Solution structure of a 2:1 quindoline-c-MYC G-quadruplex: insights into G-quadruplex-interactive small molecule drug design. J Am Chem Soc 2011;133:17673–80. https://doi.org/10.1021/ja205646q
- 66. Long W, Zheng B-X, Huang X-H et al. Molecular recognition and imaging of human telomeric G-quadruplex DNA in live cells: a systematic advancement of thiazole orange scaffold to enhance binding specificity and inhibition of gene expression. J Med Chem 2021;64:2125–38. https://doi.org/10.1021/acs.jmedchem.0c01656
- 67. Belotserkovskii BP, Liu R, Tornaletti S *et al.* Mechanisms and implications of transcription blockage by guanine-rich DNA sequences. *Proc Natl Acad Sci USA* 2010;107:12816–21. https://doi.org/10.1073/pnas.1007580107
- 68. He T-C, Sparks AB, Rago C *et al.* Identification of c-MYC as a target of the APC pathway. *Science* 1998;281:1509–12. https://doi.org/10.1126/science.281.5382.1509
- 69. Balasubramanian S, Hurley LH, Neidle S. Targeting G-quadruplexes in gene promoters: a novel anticancer strategy?. *Nat Rev Drug Discov* 2011;10:261–75. https://doi.org/10.1038/nrd3428
- Liu W, Lin C, Wu G et al. Structures of 1:1 and 2:1 complexes of BMVC and MYC promoter G-quadruplex reveal a mechanism of ligand conformation adjustment for G4-recognition. Nucleic Acids Res 2019;47:11931–42.
- Calabrese DR, Chen X, Leon EC et al. Chemical and structural studies provide a mechanistic basis for recognition of the MYC G-quadruplex. Nat Commun 2018;9:4229. https://doi.org/10.1038/s41467-018-06315-w
- 72. Feng B, Sosa RP, Mårtensson AKF *et al.* Hydrophobic catalysis and a potential biological role of DNA unstacking induced by environment effects. *Proc Natl Acad Sci USA* 2019;116:17169–74. https://doi.org/10.1073/pnas.1909122116